5084 *Chem. Mater.* **2010,** *22,* 5084–5092
DOI:10.1021/cm101642b

CHEMISTRY OF MATERIALS
Article

Photoelectrochemical and Photoresponsive Properties of Bi_2S_3 Nanotube and Nanoparticle Thin Films

Asif Ali Tahir,[§] Muhammad Ali Ehsan,[†] Muhammad Mazhar,*[,‡] K. G. Upul Wijayantha,*[,§] Matthias Zeller,[∥] and A. D. Hunter[∥]

[†]*Department of Chemistry, Quaid-I-Azam University, Islamabad-45320, Pakistan,* [‡]*Department of Chemistry, Faculty of Science, University of Malaya, Lembah Pantai, 50603-Kuala Lumpur, Malaysia,* [§]*Department of Chemistry, Loughborough University, Loughborough LE11 3TU, U.K., and* [∥]*STaRBURSTT-Cyberdiffraction Consortium at YSU and Department of Chemistry, Youngstown State University, 1 University Plaza, Youngstown, Ohio 44555-3663*

Received June 12, 2010. Revised Manuscript Received July 15, 2010

Bi_2S_3 nanotubes and nanoparticle in the form of thin films were deposited on fluorine doped SnO_2 (FTO) coated conducting glass substrates by Aerosol Assisted Chemical Vapor Deposition (AACVD) using tris-(*N*,*N*-diethyldithiocarbamato)bismuth(III), $[Bi(S_2CN(C_2H_5)_2)_3]_2$ (**1**) as a precursor. Thin films were deposited from solutions of (**1**) in either chloroform, dichloromethane, or a 1:1 mixture of chloroform and toluene at temperature between 350 to 450 °C and characterized by X-ray diffraction (XRD), UV−vis spectroscopy, field emission gun scanning electron microscopy (FEGSEM), and energy dispersive X-ray (EDX) analysis. FEGSEM images of films deposited from chloroform or dichloromethane exhibit well-defined and evenly distributed nanotubes with an average internal diameter of 40 nm. Films deposited from chloroform/toluene, on the other hand, have compact nanostuctured morphology. Bandgaps of 1.85 and 1.8 eV were estimated for nanotubes and nanoparticles, respectively, by extrapolating the linear part of the Tauc plot recorded for the films. The *n*-type Bi_2S_3 thin films display a reasonable photoactivity under illumination and are thus promising candidates for photoelectrochemical applications. The photoelectrochemical characteristics recorded under AM 1.5 illumination indicated photocurrent density of 1.9 mA/cm^2 and 1.0 mA/cm^2 at 0.23 V versus Ag/AgCl/3 M KCl for the films deposited from chloroform and chloroform/toluene, respectively. The photocurrent is among the highest reported for any Bi_2S_3 photoelectrode to date. Repeated illumination cycles show that the Bi_2S_3 thin films display a reasonable photosensitivity and response indicating their potential to be used in photodetector and optoelectronic nanodevice applications.

Introduction

Starting with the first discovery of carbon nanotubes, inorganic one-dimensional (1D) nanostructures have been at the center of attention in many areas of research from fundamental sciences to industrial systems engineering. Initial interest was targeted on the intrinsic properties of these fascinating material structures, however, the recent focus is aimed at their unusual physical and chemical properties as well as possible applications.[1,2] Inorganic nanostructures have shown great potential and applications are in the research and development of nanodevices.[3] Nanotubes and nanowires, for example, possess several different areas of contact (borders, inner and outer surfaces, and structured tube walls) that in principle can be functionalized in several ways such as by using of nanorods, tubes, and wires as, for example, nanoscale host materials.[4,5]

Binary metal chalcogenides $A_2^{V}B_3^{VI}$ (A = As, Sb, Bi; B = S, Se, Te) have drawn extensive attention as they are an important class of semiconductors that are already used in numerous technological components as, for example, photoconducting targets, electronic and optoelectronic devices,[6] thermoelectric devices,[7] hydrogen storage materials,[8,9] and sensors.[10] For application in photoelectrochemical (PEC) solar cells, the photoelectrode material should have appropriate band energetics, so that it can

*To whom correspondence should be addressed. E-mail: u.wijayantha@lboro.ac.uk (K.G.U.W.), mazhar42pk@yahoo.com (M.M.).

(1) Remškar, M. *Adv. Mater.* **2004**, *16*, 1497–1504.
(2) Patzke, G. R.; Krumeich, F.; Nesper, R. *Angew. Chem., Int. Ed.* **2002**, *41*, 2446–2461.
(3) Hu, J.; Odom, T. W.; Lieber, C. M. *Acc. Chem. Res.* **1999**, *32*, 435–445.
(4) Bao, H.; Li, C. M. X.; Cui; Song, Q.; Yang, H.; Guo, J. *Nanotechnology* **2008**, *19*, 335302.
(5) Bao, H.; Li, C. M.; Cui, X.; Gan, Y.; Song, Q.; Guo, J. *Small* **2008**, *4*, 1125–1129.
(6) Suarez, R.; Nair, P. K.; Kamat, P. V. *Langmuir* **1998**, *14*, 3236–3241.
(7) Chen, B. X.; Uher, C.; Iordanidis, L.; Kanatzidis, M. G. *Chem. Mater.* **1997**, *9*, 1655–1658.
(8) Li, L.; Sun, N.; Huang, Y.; Qin, Y.; Zhao, N.; Gao, J.; Li, M.; Zhou, H.; Qi, L. *Adv. Funct. Mater.* **2008**, *18*, 1194–1201.
(9) Zhang, B.; Ye, X.; Hou, W.; Zhao, Y.; Xei, Y. *J. Phys. Chem. B* **2006**, *110*, 8978–8985.
(10) Grigas, J.; Talik, E.; Lazauskas, V. *Phys. Status Solidi B* **2002**, *232*, 220–230.

Published on Web 08/09/2010

absorb almost the entire visible region of the solar spectrum while maintaining its structural and electronic integrity (i.e., photostable in semiconductor-electrolyte configuration).[11] Among different chalcogenide materials, bismuth sulfide (Bi_2S_3) is known to be an attractive material for PEC application as it has a reasonably low band gap (Eg = 1.7 eV), an absorption coefficient in the order of 10^4 to 10^5 cm^{-1}, and a reasonable incident photon to electron conversion efficiency (~5%).[12] Bi_2S_3 is also a promising semiconductor material for applications in photovoltaic cells[13] and thermoelectric-cooling technologies because of its environmental compatibility.[14] When composed of nanosized, particles quantum size effects also play an important role in determining the PEC performance of Bi_2S_3 electrodes, which is an added benefit for tuning light absorbance properties.[15]

With nanosized Bi_2S_3 being an attractive candidate material for optoelectronic applications, the investigation of new methods for fabrication of nanowires and nanorods of Bi_2S_3 has been extensively conducted in the last few years.[16,17] Several studies on the synthesis of Bi_2S_3 have been reported, including solventless,[18] solvothermal,[19,20] hydrothermal,[21,22] sonochemical,[23] colloidal chemistry routes,[24] surfactant-assisted approaches,[25] vapor deposition methods,[26] microwave irradiation[27] and low-pressure metal−organic chemical vapor deposition (LP-MOCVD).[28] However, all these methods suffer from high production costs, and/or require complicated manipulations and instrumentations; therefore materials scientists are working to explore more facile routes to fabricate Bi_2S_3 nanocrystallites thin films at low cost and in scalable ways.

There are several reports on the formation of Bi_2S_3 nanostructures (nanoparticles, nanorods, and nanotubes) by the hydrothermal processes but only a few reports on the use of single source precursors for growth of Bi_2S_3 nanostructured films by CVD. In fact, to the best of our knowledge there is no report on a single step deposition of Bi_2S_3 nanotubes. An example of a single-source route is carried out on the deposition of thin films of Bi_2S_3 from bismuth dithiocarbamates, $[Bi(S_2CNRR')_3]$ (R = Et, Me, R′ = hexyl) by LP-MOCVD.[28,29] The resulting films are found to be composed of nanofibers and nanorods, and no study was conducted on their physical properties or potential applications of these Bi_2S_3 thin films.

The most important requirement for a CVD process is the availability of a suitable precursor. For low-pressure (LP) CVD, volatility is a necessary requirement, and the precursor should decompose at elevated temperatures on the substrate surface to give the desired thin film. The precursor has to be readily volatile at a temperature well below its decomposition temperature. However, because of new developments in CVD systems, for example, aerosol-assisted (AA) CVD and liquid-injection (LI) CVD, this is no longer crucial.[30] Classical LP-CVD is also very specific in its operation; usually a dynamic vacuum 10^{-2} Torr or more has to be maintained throughout the deposition and has only a few variables such as substrate temperature or deposition time to control the morphology and structure of the thin films. These stringent requirements and limitations have undermined the importance and applications of LP-CVD.

Among the alternative thin film deposition techniques, aerosol-assisted chemical vapor deposition (AACVD) is a relatively simple method that is easy to conduct and very versatile. The advantages of AACVD are that a single solution source can be used to fabricate multicomponent layers ensuring both reproducibility and the presence of all the components in the deposited layer. Moreover, high quality thin films can be obtained by AACVD as the homogeneity of the aerosol can readily be controlled; the size of the aerosol droplets is closely controlled by the frequency of the ultrasonic generator. It also diminishes the volatility requirement for the precursor: it merely has to be soluble in a solvent from which an aerosol can be generated.[31,32] The composition and architecture of the films can be easily controlled via experimental parameters, such as solution concentration, solvent, nature of the carrier gas, carrier gas flow, deposition time, and substrate temperature, to name just a few. It is the multiplicity of these adjustable parameters that indicates one of the prominent advantages of AACVD techniques.

There is no report on the direct deposition of Bi_2S_3 nanotubes on a conducting substrate, or of the investigation of photoelectrochemical and photoresponsive

(11) Peter, L. M.; Riley, D. .J.; Tull, E. J.; Wijayantha, K. G. U. *Chem. Commun*. **2002**, 1030–1031.
(12) Peter, L. M.; Wijayantha, K. G. U.; Riley, D. J.; Waggett, J. P. *J. Phys. Chem. B* **2003**, *107*, 8378–8381.
(13) Miller, B.; Heller, A. *Nature* **1976**, *262*, 680–681.
(14) Liufu, S. C.; Chen, L. D.; Yao, Q.; Wang, C. F. *Appl. Phys. Lett*. **2007**, *90*, 112106.
(15) Mane, R. S.; Desai, J. D.; Joo, O.-S.; Han, S.-H. *Int. J. Electrochem. Sci*. **2007**, *2*, 141–148.
(16) Tian, L.; Tan, H. Y.; Vittal, J. J. *Cryst. Growth Des*. **2008**, *8*, 734–738.
(17) Sigman, B. M.; Korgel, B. A. *Chem. Mater*. **2005**, *17*, 1655–1660.
(18) Wang, Y.; Chen, J.; Wang, P.; Chen, L.; Chen, Y.-B.; Wu, L.-M. *J. Phys. Chem. C* **2009**, *113*, 16009–16014.
(19) Liu, Z.; Peng, S.; Xie, Q.; Hu, Z.; Yang, Y.; Zhang, S.; Qian, Y. *Adv. Mater*. **2003**, *15*, 936–940.
(20) Lou, W.; Chen, M.; Wang, X.; Liu, W. *Chem. Mater*. **2007**, *19*, 872–878.
(21) (a) Stavila, V.; Whitmire, K. H.; Rusakova, I. *Chem. Mater*. **2009**, *21*, 5456–5465. (b) Alemi, A.; Dolatyari, M. *Radiat. Eff. Defects Solids* **2008**, *163*, 123–130.
(22) (a) Shao, M. W.; Mo, M. S.; Cui, Y.; Chen, G.; Qian, Y. T. *J. Cryst. Growth* **2001**, *233*, 799–802. (b) Zhu, G. Q.; Liu, P.; Zhou, J. P.; Bian, X. B.; Wang, X.; B.; Li, J. *Chem. J. Chin. Univ.-Chin*. **2008**, *29*, 240–243.
(23) Zhu, J. M.; Yang, K.; Zhu, J. J.; Ma, G. B.; Zhu, X. H.; Zhou, S. H.; Liu, Z. G. *Opt. Mater*. **2003**, *23*, 89–92.
(24) Cademartiri, L.; Malakooti; O' Brien, R.; P. G.; Migliori, A.; Petrov, S.; Kherani, N. P.; Ozin, G. A. *Angew. Chem., Int. Ed*. **2008**, *47*, 3814–3817.
(25) Li, Q.; Shao, M. W.; Wu, J.; Yu, G. H.; Qian, Y. T. *Inorg. Chem. Commun*. **2002**, *5*, 933–636.
(26) Yu, X.; Cao, C. *Cryst. Growth Des*. **2008**, *8*, 3951–3955.
(27) Liao, X.-H.; Wang, H.; Zhu, J.-J.; Chen, H.-Y. *Mater. Res. Bull*. **2001**, *36*, 2339–2346.
(28) (a) Monteiro, O. C.; Trindade, T.; Park, J.-H.; O'Brien, P. *Chem. Vap. Deposition* **2000**, *6*, 230–232. (b) Monteiro, O. C.; Nogueira., H. I. S.; Trindade, T. *Chem. Mater*. **2001**, *13*, 2103–2111.
(29) Koh, Y. W.; Lai, C. S.; Du, A. Y.; Tiekink, E. R. T.; Loh, K. P. *Chem. Mater*. **2003**, *15*, 4544–4554.
(30) Malik, M. A.; Afzaal, M.; O'Brien, P. *Chem. Rev*. **2010**, *110*, 4417–4446.
(31) Cross, W. B.; Parkin, I. P.; O'Neill, S. A.; Williams, P. A.; Mahon, M. F.; Molloy, K. C. *Chem. Mater*. **2003**, *15*, 2786–2796.
(32) Palgrave, R. G.; Parkin, I. P. *J. Mater. Chem*. **2004**, *14*, 2864–2867.

properties of the resulting films. The objective of the present work is to apply a commonly known precursor for the deposition of Bi_2S_3 thin film by AACVD for specific applications. This led us to focus our research on two areas: the investigation of suitable molecular precursors, and its use of such precursors for the deposition of Bi_2S_3 nanostructured photoelectrodes on a target substrate such as fluorine doped SnO_2 coated glass (FTO) by AACVD process. As for the CVD process, the precursor should be stable and have a low degree of toxicity for easy to handle and storage. Ultimately, the precursor must be able to be easily synthesized, and the synthesis must be adaptable to larger scale production without major problems including cost and environmental impact.[30] Following our previous work directed toward the synthesis of metal complexes for the deposition of thin films[33,34] for PEC applications,[35,36] we selected $Bi_2[(S_2CN(C_2H_5)_2)_3]_2$ (**1**) as a precursor as it fulfills the required criteria. We, for the first time, successfully deposited Bi_2S_3 nanotubes and nanoparticles in the form of thin films on glass and FTO substrates by altering the deposition parameters and characterized the optical, photoelectrochemical, and photoresponsive properties of the deposited thin films.

Experimental Section

The precursor $Bi_2[(S_2CN(C_2H_5)_2)_3]_2$ (**1**) was synthesized according to a literature process[37] by the reaction of potassium dithiocarbamate with $Bi(NO_3)_3 \cdot 5H_2O$ in acetone. The precursor (**1**) was characterized by melting point, elemental analysis, NMR, single crystal X-ray crystallography, and thermogravimetric analysis. Details of the synthetic procedure and characterization of the precursor (**1**) are given in the Supporting Information. The precursor (**1**) is highly soluble in chloroform and dichloromethane (20 g/100 mL) while the solubility decreases to 12 g/100 mL in a 1:1 mixture of chloroform and toluene.

Deposition of Thin Films by AACVD. Thin films were deposited by AACVD on a fluorine-doped tin oxide (FTO) coated glass (1 × 2 cm) substrate (TEC 8 Pilkington, 8 Ω/square). Substrates were ultrasonically cleaned with distilled water, acetone, isopropanol, and ethanol. Details of the AACVD assembly are described elsewhere.[36] In a typical deposition a 0.05 M solution of precursor (**1**) was used to generate the aerosol at room temperature using a PIFCO air humidifier. Argon was passed through the aerosol mist at a flow rate of 150 mL/min, thus forcing the aerosol droplets into the reactor chamber. Depositions were conducted for 30 min. The exhaust from the reactor was vented directly into the extraction system of a fume cupboard. Toward the end of the experiment the aerosol line was closed, and argon was allowed to flow over the substrate and cool the films to about 40 °C before they were removed from the reaction chamber for structural and photoelectrochemical studies. The morphology and nanostructure of the thin films were controlled by altering the deposition temperature as well as by changing the solvent of the deposition solution. Thin films with well-defined nanotubes were deposited by using chloroform or dichloromethane as the deposition solvent, while compact nanostructured films were deposited from a 1:1 solvent mixture of chloroform and toluene. The AACVD experiments were repeated several times to ensure the reproducibility of thin films.

Structural Characterization. The identity of the phase and the degree of crystallinity of the deposited films were investigated using a PANalytical X-ray diffractometer model X′Pert PRO with primary monochromatic high intensity Cu−Kα (λ = 1.54184 Å) radiation. A range of 2θ (from 5.00 to 90.00) was scanned. Data on the morphology and composition of the thin films were obtained using a field emission gun scanning electron microscope (FEGSEM, Leo 1530 VP) operated at an acceleration voltage of 5.0 kV and equipped with an energy-dispersive X-ray spectroscopy (EDS) detector.

Optical and Photoelectrochemical Characterization. Room temperature UV−vis absorption spectra were recorded on a Lambda 35 Perkin-Elmer UV−vis spectrophotometer in the wavelength range of 300−1000 nm. An FTO coated glass substrate was placed in the reference optical path; thus, the absorbance spectra included the contributions only from the Bi_2S_3 films.

A homemade three-electrode electrochemical cell, fitted with a quartz window, was used for photoelectrochemical characterization. An aqueous solution of 1 M Na_2SO_3 was used as the electrolyte. The potential of the Bi_2S_3 working electrode was controlled by a potentiostat (micro-Autolab, type III). A Ag/AgCl/3 M KCl electrode was used as the reference electrode, and a Pt wire was adopted as the counter electrode. In the electrochemical cell light enters through a quartz window and travels about a 5 mm path length in the electrolyte before illuminating the photoelectrode. The Bi_2S_3 electrode was illuminated through the electrolyte side, and the illumination area was 1 cm^2. The illumination source was an AM1.5 class A solar simulator (Solar Light 16S − 300 solar simulator). The voltage scan speed was 0.01 V/s, and light was manually chopped at regular intervals to record the light and dark current simultaneously.

Measurements of Photoresponsive Properties. A photoresponse device was built by sandwiching an as-deposited Bi_2S_3 thin film on FTO on a blank FTO glass substrate with a device configuration of FTO/Bi_2S_3/FTO as shown in the inset of Figure 9. A halogen lamp (100 mW/cm^2) was used as the illumination source, and a bias voltage of 20 mV was applied on the FTO electrode. The light was interrupted at 25 s intervals, and the currents were measured at potentiostatic mode (micro-Autolab, type III). With the light regularly chopped, current spikes were recorded.

Results and Discussion

Thin Film Characterization. In AACVD process solvent plays a vital role by controlling the viscosity of the deposition solution which directly affects the droplet size of the aerosol. The polarity and specific heat capacity of the solvent are also important and play a significant role during the decomposition process in the reactor. In this work, we selected both nonpolar and polar solvents to investigate their effect on the texture, morphology, and photoelectrochemical performance of the films. The

(33) Tahir, A. A.; Mazhar, M.; Hamid, M.; Wijayantha, K.G. U.; Molloy, K. C. *Dalton Trans.* **2009**, 3674–3680.
(34) Hamid, M.; Tahir, A. A.; Mahzar, M.; Zeller, M.; Hunter, A. D. *Inorg. Chem.* **2007**, *46*, 4120–4127.
(35) Wijayantha, K. G. U.; Peter, L. M.; Otley, L. C. *Sol. Energy Mater. Sol. Cells* **2004**, *83*, 363–369.
(36) Tahir, A. A.; Wijayantha, K. G. U.; Yarahamdi, S. S.; Mazhar, M.; Mckee, V. *Chem. Mater.* **2009**, *21*, 3763–3772.
(37) Raston, C. L.; White, A. H. *J. Chem. Soc., Dalton Trans.* **1976**, 791–794.

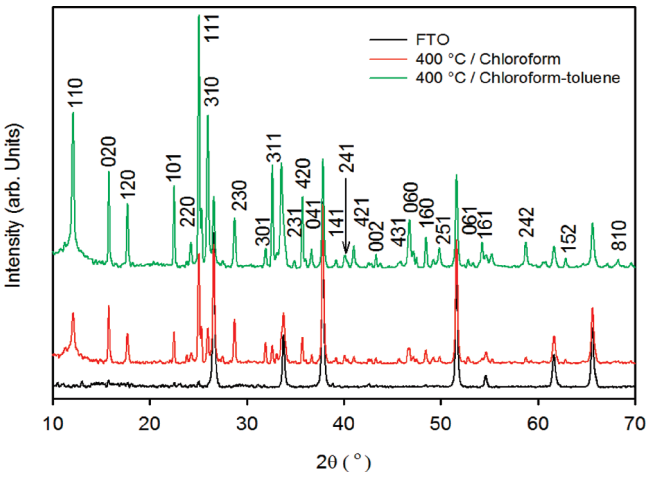

Figure 1. XRD patterns of Bi_2S_3 thin films deposited from precursor (**1**) at 400 °C on FTO substrate.

effect of solvent and deposition temperature on the properties of deposited thin films from precursor (**1**) was investigated using different solvents such as chloroform, dichloromethane, and a (1:1) mixture of chloroform and toluene at different deposition temperatures. The thin films deposited using CH_2Cl_2 as the solvent have very similar morphology as to the films deposited from $CHCl_3$ as solvent. The results presented here will focus on the structural, PEC, and photoresponsive properties of films made from chloroform and the chloroform/toluene mixtures as the solvents at different deposition temperatures. All films deposited exhibit excellent adhesion properties on the substrate FTO as verified by the "scotch tape test" and are stable in air and atmospheric moisture. Films deposited for more than 30 min with a thickness above 5 μm lose adhesion and failed the scotch tape test. Deposited films were characterized by X-ray diffraction (XRD), FEGSEM, EDX, and studied for their optical, photoelectrochemical, and photoresponsive properties.

Structural Characterization. XRD was used to study the crystallinity of the deposited films, and representative XRD peak patterns are shown in Figure 1. To eliminate the interference of SnO_2 from the FTO substrate, the films were also deposited on plane glass under similar deposition conditions as for the FTO substrates (see Supporting Information, Figure S1). The XRD diffractogram for FTO is also shown in Figure 1 to distinguish the FTO peaks. Comparison of the XRD pattern of the deposited thin films with the standard for Bi_2S_3 [00-017-0320][38] revealed that the crystalline product formed is pure Bi_2S_3 in its orthorhombic stibnite type modification, crystallizing in the *Pbnm* (62) space group.[39] The XRD patterns of the nanotubes (Figure 1) show no significant deviation in relative peak intensities from that of bulk bismuthinite. However, the diffraction patterns for the nanoparticles (Figure 1) exhibit some preferred orientation with higher (310) peak intensity as compared to the nanotube films deposited from chloroform as solvent.

The XRD peak patterns show no signs of any chemically or pyrolytically driven phases other than Bi_2S_3 in the film. The XRD results agree well with reported data of Bi_2S_3 nanostructures deposited from bismuth dithiocarbamate precursor using other techniques.[28,29] In contrast, Waters et al.[40] showed that the film composition deposited by AACVD using $Bi[(SPR_2)_2N]_3$ (R = ^{i}Pr or Ph) precursors are highly dependent on carrier gas flow and temperature. Notably, the Bi/S ratio in the films changes with the change in carrier gas flow and deposition temperature. The films also contain traces of phosphorus as an impurity. Similarly, Koh et al.[29] had only been able to deposit pure Bi_2S_3 thin films for short deposition times from bismuth xanthate precursors. At increased deposition times they observed crystalline phases corresponding to elemental monoclinic sulfur forming on the surface of the resulting thicker Bi_2S_3 films. Interestingly, no such phases were detected in the present study for the films deposited by AACVD even after prolonged deposition times when the films were grown up to 30 μm as shown by SEM cross-sectioning. (Supporting Information, Figure S4). Energy dispersive X-ray spectra (EDX) were also obtained to determine the stoichiometric composition of the thin films, indicating that the thin films are composed of pure Bi_2S_3. The molar ratio of Bi/S obtained from the peak areas of the EDX graph is 39.45:60.55 and thus close to the expected 2:3 ratio of Bi_2S_3. The XRD and EDX results also prove the advantage of precursor (**1**) over the other bismuth precursors used for the deposition of Bi_2S_3 thin films.

Surface Characterization. The morphology and structure of the Bi_2S_3 films were investigated by field emission gun scanning electron microscopy (FEGSEM). Typical SEM images of the thin films prepared using chloroform as a deposition solvent at three different deposition temperatures (350, 400, and 450 °C) are presented in Figure 2. The results illustrate that the films have complex nanostructures composed of nanotubes grown vertical on the FTO substrate as illustrated by the cross-sectional SEM image in Figure 2d. The topographical SEM image of the film deposited at 350 °C (Figure 2a) shows that the film consists of randomly oriented nanorods with a length of 200−400 nm. The image also indicates that some of the tubes started growing upward. The films deposited at 400 °C (Figure 2b) indicate formation of much larger and hollow nanotubes growing upward from the FTO surface. Remarkably the nanotubes grew more than a micrometer in length without any signs of fractures or breaking. The tubes have an internal diameter of 40 nm as shown in the high resolution image in the inset of Figure 2d. The films deposited at 450 °C are composed of radially oriented nanowires/tubes with a diameter of 50−70 nm and an ultralong length of tens of micrometers (Figure 2c). The image also shows that the nanowires/tubes are coiled together yielding a random and highly porous structure at the surface of the thin film. Bao et al.[5] showed that such

(38) (a) ICCD powder diffraction database file card number [00-017-0320]. (b) Swanson, H. E.; et al. *Natl. Bur. Stand.* **1953**, *4*, 23.
(39) Hofmann, W. *Z. Kristallogr.* **1933**, *84*, 177–178.
(40) Waters, J.; Crouch, D.; Raftery, J.; O'Brien, P. *Chem. Mater.* **2004**, *16*, 3289–3298.

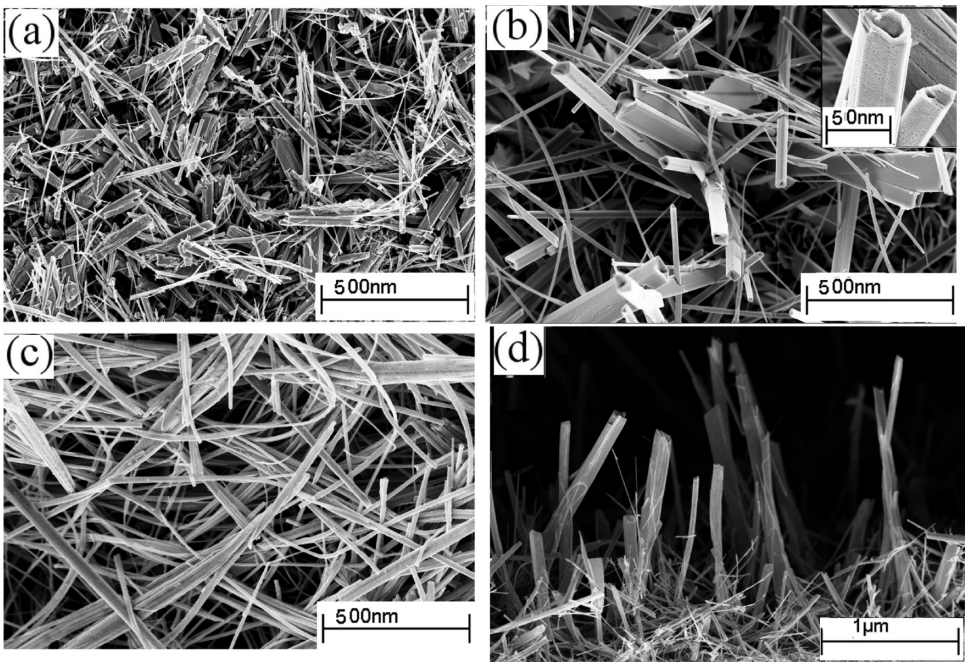

Figure 2. Surface topography of Bi_2S_3 thin films deposited on FTO substrate using chloroform as a solvent at (a) 350 °C, (b) 400 °C, (c) 450 °C, and (d) cross-section of film deposited at 400 °C; Inset of (b) shows a high resolution image of a nanotube.

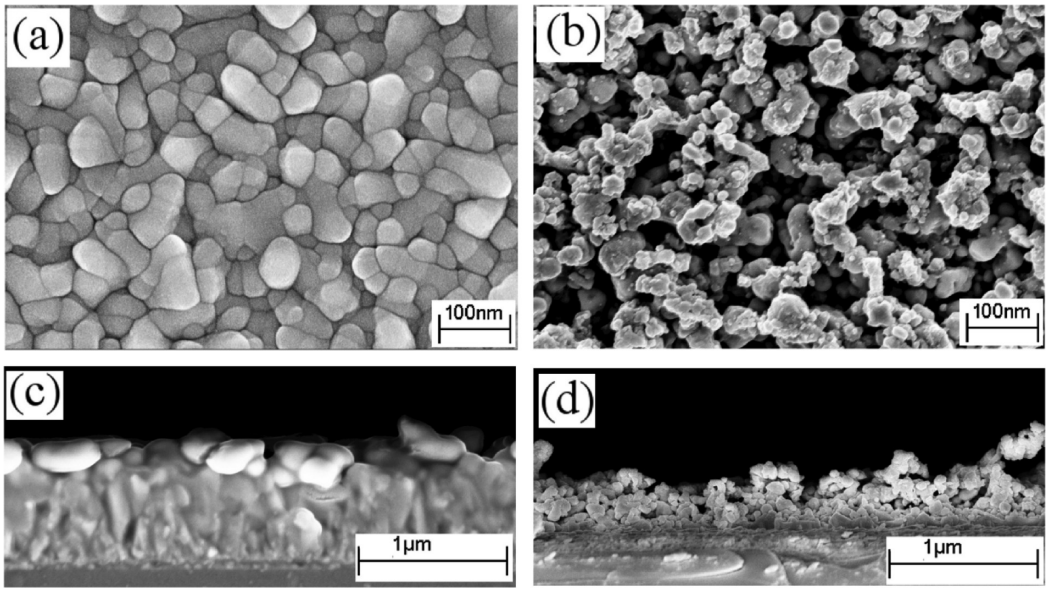

Figure 3. SEM images of the Bi_2S_3 surface topography of thin films deposited on the FTO substrate using chloroform/toluene (1:1) as the solvent at (a) 400 °C and (b) 450 °C, (c) and (d) show the cross sections of films deposited at 400 and 450 °C, respectively.

types of nanowires can be used in back-to-back Schottky diodes. They have also shown that I−V characteristics of nanowires exhibit a unique rectifying behavior, indicating potential applications in electronic nanodevices. Such locally ordered nanowire structures can also be used for fabricating nanosize optoelectronic and thermoelectric devices and may serve as nanoreactors and hosts.[41]

The films deposited by using a mixture of chloroform and toluene (1:1) exhibit a completely different morphology as shown in Figure 3. The films deposited at 350 and 400 °C are very compact nanostructured with a particle size ranging from 25 to 45 nm as shown in Figure 3a and have an excellent adhesion to the FTO substrate. A cross-section (Figure 3c) shows the thickness of the film to be about 600 nm. (Differentiation between the FTO substrate and the Bi_2S_3 layer is difficult because of the compact nature of the film). Films deposited at 450 °C show a porous structure and are composed of spherically shaped well-defined grains of 30−50 nm size (Figure 3b and 3d).

The formation of films with different morphology and structure with the change of deposition solvent can be explained on the basis of homogeneous and heterogeneous

(41) Shen, X.-P.; Yina, G.; Zhang, W.-L.; Xu, Z. *Solid State Commun.* **2006**, *140*, 116–119.

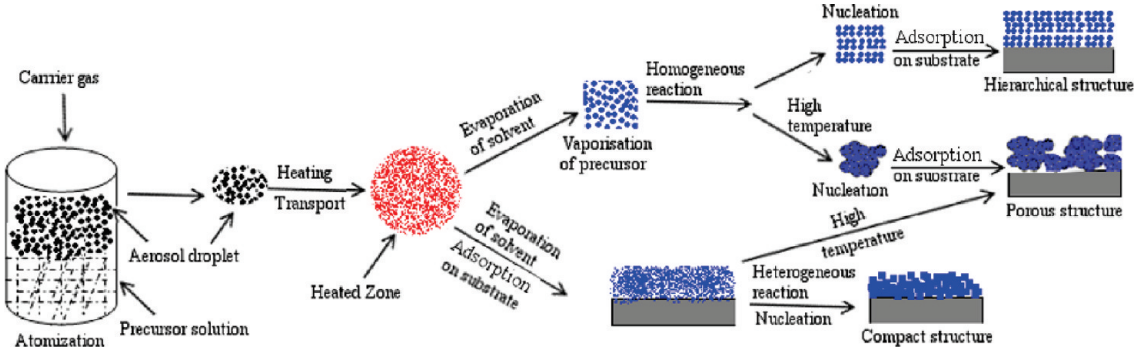

Figure 4. Schematic representation of AACVD process for the deposition of thin films.

chemical reactions and nucleation that constitute the CVD process.[42] The main processes commonly occurring in AACVD are schematically described in Figure 4. In the first step the aerosol is delivered into the heated zone, where the solvent evaporates and vaporization of the precursor starts. The vaporized precursor then undergo subsequent decomposition in the gas phase (homogeneous) or on the heated substrate (heterogeneous) to deposit the desired film. The formation of thin films in the AACVD process is the result of homogeneous or heterogeneous reaction or a combination of both homogeneous nucleation in the gas phase and heterogeneous growth on the substrates. The type and ratio between the homogeneous and the heterogeneous processes are directly responsible for the morphology, structure, and composition of the thin films.[43] The balance between homogeneous and heterogeneous reaction in the AACVD process can be adjusted by tuning the deposition parameters, such as the preheating temperature, the substrate temperature, the carrier gas flow rate, the type of solvent, and also the concentration of precursor solution. These parameters determine the type of chemical reaction by controlling the chemical kinetics and thermodynamics of the deposition process which directly influence the structure, morphology, and composition of the resulting thin films.[44] Keeping all other parameters constant, composition, morphology, and nanostructure of the thin films can be controlled by selecting solvents with a different specific heat capacity. The change in the solvent composition influences the nature of the deposition reaction by changing the size and thermodynamics of the aerosol droplets. In the current work, the concept of homogeneous and heterogeneous deposition reaction is maintained to deposit Bi_2S_3 thin films with different morphology and nanostructure by tuning the solvent of the deposition solution. Chloroform, a low specific heat capacity solvent, facilitates homogeneous reaction during deposition by evaporating and leaving the precursor molecules to vaporize much earlier in the heated zone. In a homogeneous reaction, the vaporization and decomposition of the precursor starts in the gaseous phase followed by the nucleation to form Bi_2S_3 particles. These particles are then adsorbed on the substrate surface, and a ripening/growing process leads to the formation of nanotubes. Addition of toluene (a high specific heat capacity solvent), on the other hand, increases the vaporization temperature of the aerosol droplets and promotes the heterogeneous reaction. In a heterogeneous reaction, the vaporized precursor and its gaseous intermediate species are adsorbed onto the surface of the heated substrates, where they undergo substantial decomposition and chemical reactions to produce compact dense Bi_2S_3 thin films. At relatively higher deposition temperatures (~450 °C), the formation of porous Bi_2S_3 films is a result of a combined contribution of homogeneous nucleation in the gas phase and heterogeneous growth on the substrates. We assume that the solvent only contributes to change the enthalpy of the system and not the decomposition pathway of the precursor. The absence of halide contaminations in the EDX analysis of thin films indicates that the solvent is not taking part in the decomposition process and completely evaporates before the precursor decomposition starts.

Optical Properties of Bi_2S_3 Thin Films. The optoelectronic properties of semiconducting materials are crucial for a large number of applications as many unique electronic properties result from the band energy structures of semiconducting materials. In the band theory approach the band structure of solids is a function of a three-dimensional wave vector (k) within the Brillouin zone. The latter depends on the crystal structure and corresponds to the unit cell of the reciprocal lattice. The simplest method for probing the band structure of a semiconducting material is to measure its optical absorption spectrum. Figure 5 shows the absorption spectra recorded at room temperature using SnO_2 as reference to eliminate the contribution of the FTO substrate. The recorded optical spectrum was used to calculate the bandgap energy of bismuth(III) sulphide. Fermi's golden rule for fundamental interband electronic transitions was used for the relation between absorption coefficient and photon energy[45] (which is a quite reasonable approximation for values of k near the absorption edge):

$$\alpha h\nu = A_0(h\nu - E_g)^n \quad (1)$$

(42) Hou, X.; Choy, K.-L. *Chem. Vap. Deposition* **2006**, *12*, 583–596.
(43) Kodas, T. T.; Hampden-Smith, M. J. *The Chemistry of Metal CVD*; VCH: Weinheim, 1994,
(44) Choy, K. L. *Prog. Mater. Sci.* **2003**, *48*, 57–170.
(45) Marder, M. P. *Condensed Matter Physics*; John Wiley &Sons: New York, 2000; p 588.

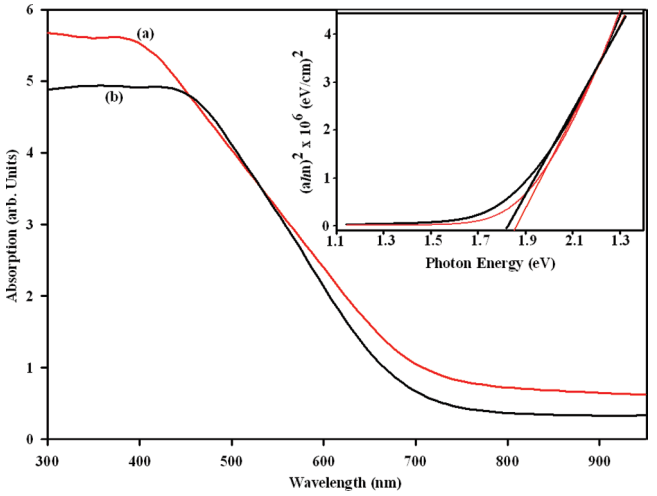

Figure 5. Optical absorption spectrum of Bi_2S_3 films deposited from precursor (**1**) by using chloroform (a) and choloroform/toluene (b) as solvents at 400 °C. Inset: Tauc plot showing the estimated optical bandgap of 1.85 and 1.8 eV, respectively.

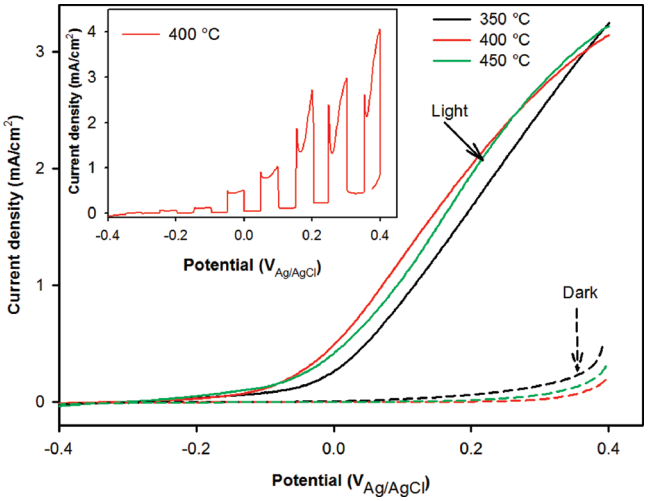

Figure 6. Current−voltage characteristics for the Bi_2S_3 thin films deposited from chloroform at deposition temperatures between 350−450 °C and measured in 1 M Na_2SO_3 electrolyte. The inset shows the photocurrent transients for the film deposited at 400 °C.

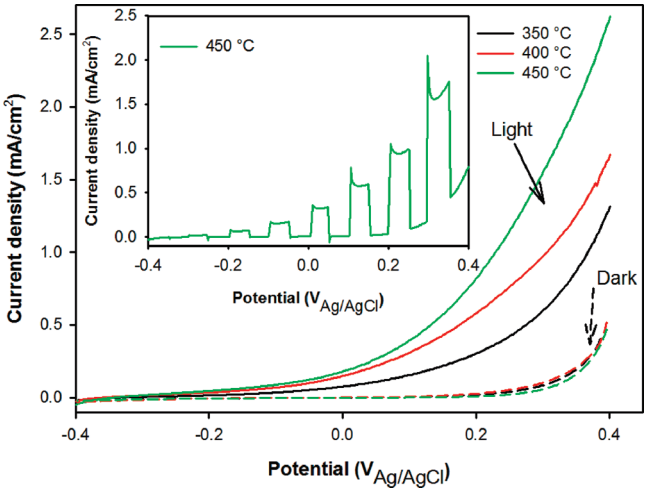

Figure 7. Current−voltage characteristics for the Bi_2S_3 thin films deposited from chloroform/toluene at a deposition temperature between 350−450 °C and recorded in 1 M Na_2SO_3 electrolyte. The inset shows the photocurrent transients for the film deposited at 450 °C.

where E_g is the bandgap, $h\nu$ is the incident photon energy, and n depends on the nature of transitions and has the values 1/2 and 2 for allowed direct and indirect transitions, respectively. It is possible to determine the nature of transitions involved by plotting the graphs of $(\alpha h\nu)^n$ versus $h\nu$ for different values of "n" as described above. The bandgap is estimated from the intercept of the extrapolated linear fit to the experimental data of the Tauc plot. A bandgap of 1.85 and 1.8 eV was estimated by extrapolating the linear part of the graph as shown in Figure 5 (inset) for the films deposited at 400 °C from chloroform and choloroform/toluene, respectively. The estimated bandgaps were found to be very close to reported values for Bi_2S_3 thin films.[15,46] The higher value of the bandgap energy when compared with the corresponding bulk value (1.7 eV) can be attributed to the nanocrystalline nature of the thin films.[47]

Photoelectrochemical Properties. The photoelectrochemical properties of Bi_2S_3 nanotube and nanoparticle thin film electrodes were studied in a three electrode mode using 1 M Na_2SO_3 as the hole scavenger. Electrodes were illuminated from the electrode side. The $J-V$ plots of thin films deposited from chloroform and chloroform/toluene at different temperatures are shown in Figure 6 and 7 respectively. For electrodes deposited from both solvents the anodic photocurrent steeply increases with the increase of applied potential and does not reach saturation which is typical for many nanoparticle electrodes. This was thought to be a result of high recombination of photogenerated charges. Similar PEC behavior was reported for colloidal Bi_2S_3 nanoparticles[48] and for electrodeposited Bi_2S_3 thin films. The observation that the photocurrent falls to zero at potentials positive to the recorded flatband potential indicates that electron accumulation decreases the photogenerated charge separation as a result of the back reaction of electrons in the conduction band (CB) with holes in the valence band (VB). For the electrodes deposited using chloroform at a deposition temperature of 400 °C the maximum photocurrent density of 1.9 mA/cm^2 was recorded (at 0.23 V vs Ag/AgCl/3 M KCl). The photocurrent slightly decreases with increase of deposition temperature which may be due to increased recombination with the increase of thickness in the film as revealed by the cross-sectional SEM image (Figure 2). The Bi_2S_3 electrodes deposited from chloroform/toluene at 450 °C show a maximum photocurrent density of 1.0 mA/cm^2 (at 0.23 V vs Ag/AgCl/3 M KCl) which is significantly lower than the recorded value for the nanotube electrodes. The photocurrent recorded for the photoelectrodes deposited from precursor (**1**) is among the highest reported to date for Bi_2S_3 electrodes.[48,49] We tentatively attribute this to the high surface area of the

(46) Han, Q.; Chen, J.; Yang, X.; Lu, L.; Wang, X. *J. Phys. Chem. C* **2007**, *111*, 14072–14077.
(47) Pejova, B.; Grozdanov., I. *Mater. Chem. Phys.* **2006**, *99*, 39–49.
(48) Riley, D. J.; Waggett, J. P.; Wijayantha, K. G. U. *J. Mater. Chem.* **2004**, *14*, 704–708.

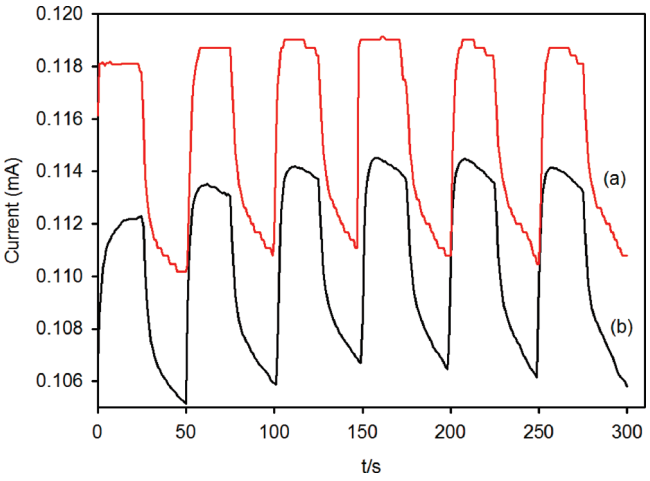

Figure 8. Sensitivity of the photoresponse at a bias of 20 mV for Bi_2S_3 thin films deposited by using chloroform (a) and chloroform/toluene (b) at 400 °C.

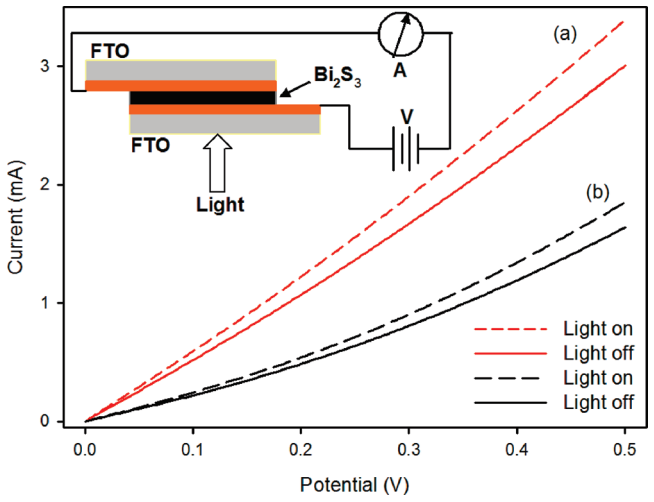

Figure 9. $I-V$ curves for Bi_2S_3 thin films deposited by using chloroform (a) and chloroform/toluene (b) at 400 °C. Inset: experimental setup for measurements of photoresponsive properties of Bi_2S_3 thin films.

nanotube electrodes. The dark current characteristics for both types of electrodes are similar. Photocurrent transients are shown in the inset of Figures 6 and 7. Strong photocurrent spikes are observed in the depletion region for electrodes deposited from chloroform indicating recombination properties of nanotube electrodes presumably because of surface states related to the high surface area. However, it shows the potential of Bi_2S_3 nanotube electrodes in PEC applications compared to nanoparticle electrodes provided that the surface recombination can be minimized. Similarly, Mohapatra et al. has shown the advantage of the use of nanotubes based electrodes in PEC applications. They found that Fe_2O_3 nanotubes are better catalysts for the photooxidation of water to H_2 and O_2 compared to other Fe_2O_3 architectures and that charge transport properties of the nanotubes are 40−50 times higher than those of the nanoparticles, which led to better photoacurrent of nanotubes based electrodes compared to that of nanoparticles electrodes.[50]

Photoresponsive Characterization. Other important applications of photoresponsive semiconductor materials are photodetectors and optical switches. They are vital elements in light wave communications, optoelectronic circuits, and imaging techniques.[51] Studies were extended in this direction in the present work to explore the applicability of Bi_2S_3 nanotube and nanoparticle thin film electrodes in photodetectors. Figure 8 shows the photoresponse of FTO/Bi_2S_3/FTO devices as a function of time. Regular chopping of the illuminated light (halogen lamp) produced a reproducible photoresponse of the device thus indicating that the Bi_2S_3 nanotube based device can be reversibly switched on and off between low and high conductivity. The on/off sensing cycles could be repeated over a period of 2 h without any noticeable deterioration. The photocurrent produced for the Bi_2S_3 nanotube based photodetector is higher than that of the Bi_2S_3 nanoparticle based device (Figure 8a,b), indicating that the conductivity of the nanotube based thin films is more sensitive to the light exposure than the nanoparticle based films. The energy from the light promotes electrons from the valence band Bi_2S_3 into the conduction band, increasing the charge carrier concentration via direct electron−hole pair creation and thus enhancing the conductivity.[52] The rise and decay time of the Bi_2S_3 switches are less than 2 ms, suggesting that the Bi_2S_3 nanotubes/particles network thin films can be used in optoelectronic switches. It is worth noting that the repeatable measurements were recorded under open-air conditions, suggesting that Bi_2S_3 thin films prepared in this work have a higher photostability than that of previously reported Bi_2S_3 nanowires which needed to be tested for photoconductivity under vacuum[53] or in a nitrogen atmosphere.[54] The photoconductivity characteristics suggest that Bi_2S_3 nanowires are good candidates for optoelectronic switches.[55]

The $I-V$ curves of the FTO/Bi_2S_3/FTO devices measured for a 0.5 V bias range under light and dark conditions are shown in Figure 9. The current−voltage curve for the FTO/Bi_2S_3 nanotubes based films shows that under light conditions the slope of the $I-V$ curve is higher than under dark conditions (Figure 9a), indicating an enhanced conductivity upon irradiation. A similar increase of the slope of the $I-V$ curve was also seen for the FTO/Bi_2S_3 nanoparticles based films (Figure 9b) but with a less significant response when compared with that of the nanotube based films. These results confirm that the conductivity of the nanotubes is more sensitive than that of the nanoparticles. Interestingly, the $I-V$ curves

(49) (a) Mane, R. S.; Sankapal, B. R.; Lokhande, C. D. *Mater. Chem. Phys.* **1999**, *60*, 158–162. (b) Mane, R. S.; Sankapal, B. R.; Lokhande, C. D. *Mater. Chem. Phys.* **1999**, *60*, 196–203.
(50) Mohapatra, S. K.; John, S. E.; Banerjee, S.; Misra, M. *Chem. Mater.* **2009**, *21*, 3048–3055.
(51) Yu, X. L.; Cao, C. B. *Cryst. Growth Des.* **2008**, *8*, 3951–3955.
(52) Li, L.; Cao, R.; Wang, Z.; Li, J.; Qi, L. *J. Phys. Chem. C* **2009**, *113*, 18075–18081.
(53) Wang, H.; Zhu, J. J.; Zhu, J. M.; Chen, H. Y. *J. Phys. Chem. B* **2002**, *106*, 3848–3854.
(54) Peng, X. S.; Meng, G. W.; Zhang, J.; Zhao, L. X.; Wang, X. F.; Wang, Y. W.; Zhang, L. D. *J. Phys. D: Appl. Phys.* **2001**, *34*, 3224–3228.
(55) Kind, H.; Yan, H. Q.; Messer, B.; Law, M.; Yang, P. D. *Adv. Mater.* **2002**, *14*, 158–160.

for both dark current and photocurrent exhibit an approximately linear shape with a bias from 0 to 0.5 V that displays ohmic behavior. These phenomena are different from the observed for individual Bi_2S_3 nanowires across two Au electrodes.[56] These results further suggest that the prepared Bi_2S_3 thin films are good candidates for applications in high-sensitivity photodetectors and photoelectronic switches. It is important to note that the Bi_2S_3 nanotube array was spontaneously formed via a facile AACVD approach and that this approach did not require any template or surfactant to control the orientation of the nanotubes, which may offer the potential for monolithic low-cost large-scale integration with CMOS electronics.[57]

Conclusions

Thin films of Bi_2S_3 nanotubes and nanoparticles can be easily grown onto FTO-coated glass by AACVD using $[Bi(S_2CN(C_2H_5)_2)_3]_2$ (**1**) as the precursor. The XRD analysis of the thin films confirms the formation of nanocrystalline Bi_2S_3. SEM studies revealed that films deposited using chloroform or dichloromethane as the solvent have morphology with well-defined nanotubes, while the films deposited using chloroform/toluene as the solvent have compact nanoparticle morphology. The photoelectrochemical characteristics recorded under AM 1.5 illumination exhibited photocurrent density of 1.9 mA/cm^2 and 1.0 mA/cm^2 at 0.23 V versus Ag/AgCl for the films deposited from chloroform and chloroform/toluene, respectively. The PEC data suggest that Bi_2S_3 nanotube thin films are promising for potential photoelectrochemical applications. The photoswitchable conductivity of films made from Bi_2S_3 nanotubes and nanoparticles shows that the films may be suitable for applications in photodetectors and photoelectronic switches. Fabrication and charge transport properties of devices based on Bi_2S_3 nanotube arrays are currently under further investigation.

Acknowledgment. K.G.U.W., M.M., A.A.T., and M.A.E. acknowledge the British Research Council and the Pakistan Science Foundation (PSF) for research co-operation grants (Loughborough University − Quaid-i-Azam University) through the "Prime Minister's Initiative for International Education 2 (PMI2)" scheme. The Smart Apex diffractometer was funded by NSF Grant 0087210, by Ohio Board of Regents Grant CAP-491, and by YSU. This work is also partly funded by EPSRC (EP/F057342/1).

Supporting Information Available: Additional information as noted in the text. This material is available free of charge via the Internet at http://pubs.acs.org.

(56) Bao, H. F.; Cui, X. Q.; Li, C. M.; Gan, Y.; Zhang, J.; Guo, J. *J. Phys. Chem. C* **2007**, *111*, 12279–12283.
(57) Konstantatos, G.; Levina, L.; Tang, J.; Sargent, E. H. *Nano Lett.* **2008**, *11*, 4002–4006.